

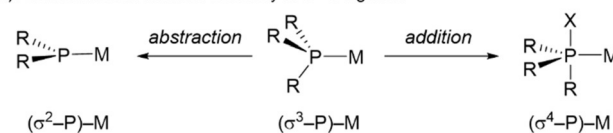
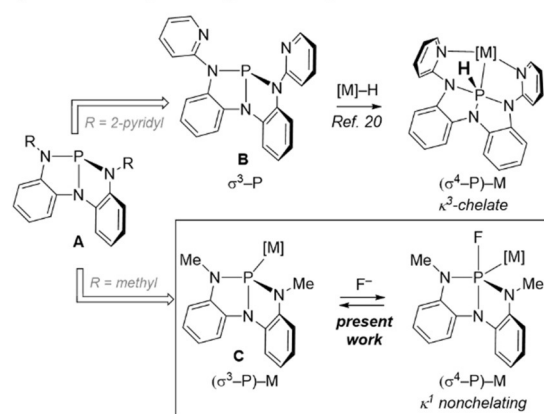
A Nontrigonal Tricoordinate Phosphorus Ligand Exhibiting Reversible “Nonspectator” L/X-Switching

Gregory T. Cleveland and Alexander T. Radosevich*

Abstract: We report here a “nonspectator” behavior for an unsupported L-function σ^3 -P ligand (i.e. $P[N(o-NMe-C_6H_4)_2]$, **1a**) in complex with the cyclopentadienyliron dicarbonyl cation (Fp^+). Treatment of **1a**· Fp^+ with $[(Me_2N)_3S][Me_3SiF_2]$ results in fluoride addition to the P-center, giving the isolable crystalline fluorometallophosphorane **1a**^F· Fp that allows a crystallographic assessment of the variance in the Fe–P bond as a function of P-coordination number. The nonspectator reactivity of **1a**· Fp^+ is rationalized on the basis of electronic structure arguments and by comparison to trigonal analogue $(Me_2N)_3P \cdot Fp^+$ (i.e. **1b**· Fp^+), which is inert to fluoride addition. These observations establish a nonspectator L/X-switching in $(\sigma^3-P)-M$ complexes by reversible access to higher-coordinate phosphorus ligand fragments.

Tricoordinate phosphorus (σ^3 -P) compounds are archetypal donor ligands in coordination chemistry.^[1–3] Within the covalent bond classification,^[4,5] σ^3 -P compounds are designated L-function ligands for transition metals (M) and are overwhelmingly construed as inert, ancillary, spectator ligands within $(\sigma^3-P)-M$ complexes. A rich “nonspectator” reaction chemistry of metal-bound σ^3 -P compounds, however, belies this prevailing view. Abstraction of a P-substituent from $(\sigma^3-P)-M$ complexes accesses dicoordinate phosphorus ligands (Figure 1a; σ^2-P^- , phosphide; σ^2-P^+ , phosphonium),^[6] and the σ^2-P^-/σ^3-P interconversion has been the focus of extensive stoichiometric^[7–13] and catalytic^[14] investigation. By complement, addition of an exogenous nucleophile to phosphorus in an L-function $(\sigma^3-P)-M$ complex increases the P-coordination number, resulting in a “metallophosphorane” complex with an X-function $(\sigma^4-P)-M$ formula.^[15] Literature concerning the addition of a P-substituent to $(\sigma^3-P)-M$ complexes to give higher-coordinate phosphorus congeners is comparatively sparse.^[16] Verkade has postulated that fluoride addition to Pd^{II} -(bis)phosphines induces $Pd^{II} \rightarrow Pd^0$ reduction via initial addition of F^- to P.^[17] Further, Nakazawa and Miyoshi have shown the possibility of nucleophilic substitution of P-substituents in cationic Fe^{II} -phosphite complexes, in some cases leading to persistent $(\sigma^4-P)-M$ products.^[18,19]

Recently, a κ^3 -chelate containing a nontrigonal σ^3 -P center (Figure 1, **B**) was shown to access directly a $(\sigma^4-P)-M$

a) Abstraction and addition reactivity of σ^3 -P ligandsb) Nonspectator reactivity of nontrigonal σ^3 -P ligandsFigure 1. Nonspectator modes of reactivity for $(\sigma^3-P)-M$ complexes.

metallophosphorane by formal insertion to a $Ru-H$ bond.^[20] An interpretation of XANES data for **B** and related compounds **A** attributed the propensity of the phosphorus center to attain higher coordination to the presence of a low-energy P-based orbital made accessible by the nontrigonal local environment.^[21] The presence of the low-lying P-centered orbital in **A** and related compounds raised the prospect of accentuated intermolecular electrophilic reactivity of such nontrigonal σ^3 -P ligands. We report here the reversible addition of an exogenous nucleophile to the P-center of an unsupported $(\sigma^3-P)-M$ complex **C** that demonstrates a nonspectator behavior of ligands **A**. With this study, direct experimental evidence is provided that delineates: (1) the inherent electronic impact on metal-binding arising from nontrigonal distortion of σ^3 -P ligands without convolution from chelate effects, and (2) the direct crystallographic observation of a nonspectator phosphorus ligand in a higher-coordinate state following exogenous nucleophile addition. The ability for nontrigonal σ^3 -P ligands to reversibly expand local coordination number while remaining σ -bound in the primary ligand sphere of a metal complex forecasts emerging opportunities for functional nonspectator ligands within $(\sigma^3-P)-M$ complexes.^[22]

On the basis of precedent from Martin^[23] and Nakazawa and Miyoshi,^[18,19] the cyclopentadienyliron dicarbonyl cation (Fp^+) was selected as a coordinatively saturated “ancillary metal”^[24] fragment for study. Iron complexes **1a**· Fp^+ and

[*] G. T. Cleveland, A. T. Radosevich

Department of Chemistry, Massachusetts Institute of Technology
77 Massachusetts Avenue, Cambridge, MA 02139 (USA)
E-mail: radosevich@mit.eduSupporting information and the ORCID identification number(s) for the author(s) of this article can be found under <https://doi.org/10.1002/anie.201909686>.

$1b \cdot Fp^+$ were prepared by ligand exchange of $[thf \cdot Fp][PF_6]^{[25]}$ with $P[N(o-NMe-C_6H_4)_2]$ (**1a**)^[26,27] and $(Me_2N)_3P$ (**1b**), respectively (Figure 2).

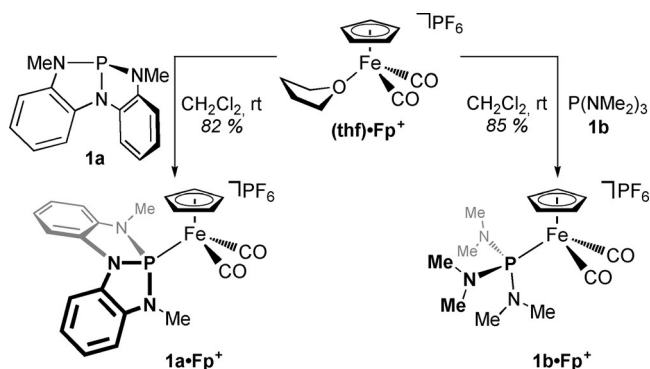


Figure 2. Synthesis of $[R_3P \cdot Fp][PF_6]$ complexes, where $R_3P = 1a$ or $1b$.

According to IR spectroscopy, the CO stretching frequencies of $1a \cdot Fp^+$ ($\nu_{asym} = 2017 \text{ cm}^{-1}$, $\nu_{sym} = 2061 \text{ cm}^{-1}$) are higher in energy than those of $1b \cdot Fp^+$ ($\nu_{asym} = 2000 \text{ cm}^{-1}$, $\nu_{sym} = 2045 \text{ cm}^{-1}$). This trend tracks qualitatively with the J_{Se-P} coupling constants for phosphorus selenides **1a**-Se ($J_{Se-P} = 907 \text{ Hz}$) and **1b**-Se ($J_{Se-P} = 784 \text{ Hz}$), suggesting to a first approximation that **1a** is a weaker σ -donor than **1b** (see Table 1 for collected metrical data). The ^{57}Fe NMR chemical shifts (obtained indirectly by 2D Fe–P correlation solution NMR experiments due to the low receptivity of the ^{57}Fe nucleus^[28]) for $1a \cdot Fp^+$ ($\delta = 616 \text{ ppm}$) and $1b \cdot Fp^+$ ($\delta = 688 \text{ ppm}$) are consistent with this interpretation, based on trends established for related cyclopentadienyliron complexes.^[29]

Further distinctions between $1a \cdot Fp^+$ and $1b \cdot Fp^+$ are manifest in structural analyses based on X-ray diffractometry data obtained with single-crystalline samples (Figure 3). Most evidently, compound $1a \cdot Fp^+$ features a shorter Fe–P bond length ($d_{Fe-P} = 2.1809(4) \text{ \AA}$) as compared to compound $1b \cdot Fp^+$ ($d_{Fe-P} = 2.2381(5) \text{ \AA}$). Also, consistent with the aforementioned vibrational data, the average Fe–C_{CO} bond length in $1a \cdot Fp^+$ ($d_{Fe-C} = 1.7886(17) \text{ \AA}$) is slightly longer than in $1b \cdot Fp^+$ ($d_{Fe-C} = 1.7766(19) \text{ \AA}$). A further feature of note concerns the dihedral angles $\phi(N-P-Fe-N)$; by projection down the P–Fe axis (Figure 3 A, right), compound $1a \cdot Fp^+$ shows a span of dihedral angles $\Omega(\phi) = 28.11(26)^\circ$, with a maximum dihedral of $\phi(N_2-P-Fe-N_3) = 137.95(13)^\circ$. By contrast, compound

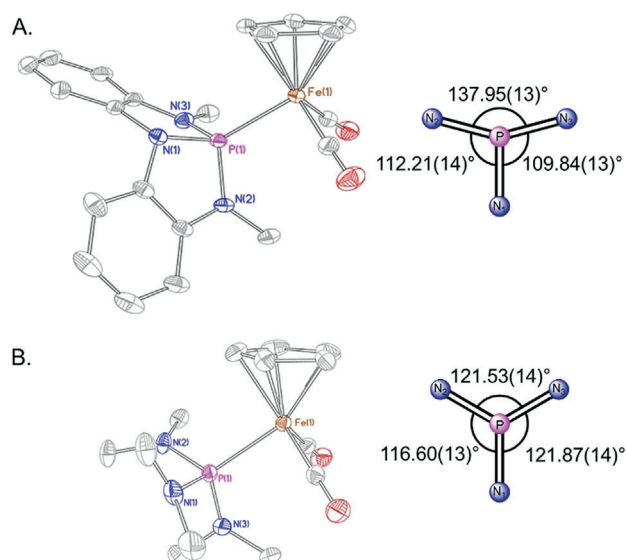


Figure 3. A) Left: Thermal ellipsoid plot for $1a \cdot Fp^+$ rendered at 50% probability level. Hydrogen atoms, noncoordinating PF_6^- counterion, and a THF solvent molecule are omitted for clarity. Selected metrical data for $1a \cdot Fp^+$: $d(Fe-P)$: 2.1809(4) Å, $d(Fe-(CO)_1)$: 1.7879(17) Å, $d(Fe-(CO)_2)$: 1.7893(16) Å, $\angle(N_1-P-N_2)$: 93.42(6)°, $\angle(N_1-P-N_3)$: 93.04(7)°, $\angle(N_2-P-N_3)$: 116.39(7)°. Right: Schematic projection down the P–Fe axis for $1a \cdot Fp^+$ illustrating dihedral angles $\phi(N-P-Fe-N)$. B) Left: Thermal ellipsoid plot for $1b \cdot Fp^+$ rendered at 50% probability level. Only one of two molecules in the asymmetric unit is depicted. Hydrogen atoms and a noncoordinating PF_6^- counterion are omitted for clarity. Selected metrical data for $1b \cdot Fp^+$: $d(Fe-P)$: 2.2381(5) Å, $d(Fe-(CO)_1)$: 1.7739(19) Å, $d(Fe-(CO)_2)$: 1.7792(18) Å, $\angle(N_1-P-N_2)$: 101.59(8)°, $\angle(N_1-P-N_3)$: 105.03(9)°, $\angle(N_2-P-N_3)$: 107.09(9)°. Right: Schematic projection down the P–Fe axis for $1b \cdot Fp^+$ illustrating dihedral angles $\phi(N-P-Fe-N)$. See Supporting Information for full details.

$1b \cdot Fp^+$ shows only a span of dihedral angles $\Omega(\phi) = 5.3(3)^\circ$ and a maximum dihedral of $\phi(N_1-P-Fe-N_3) = 121.87(14)^\circ$. These metrics illustrate the enhanced nontrigonal local geometry about phosphorus for $1a \cdot Fp^+$ as compared to $1b \cdot Fp^+$, consistent with the structural distinctions between the free ligands.^[26] For reference, the N_2-P-N_3 bond angle of $1a \cdot Fp^+$ ($116.40(7)^\circ$) is almost unchanged from that of **1a** ($115.21(7)^\circ$), showing that complexation does not significantly perturb the phosphorus triamide framework.

In an effort to parse the σ - and π -contributions to the Fe–P bonding interactions in $1a \cdot Fp^+$ and $1b \cdot Fp^+$, an energy partitioning into pairwise orbital interactions between σ^5 -P ligand (**1a** and **1b**, respectively) and Fp^+ fragments was

Table 1: Collected spectroscopic, structural, and computational data for compounds **1a**, **1b**, $1a \cdot Fp^+$, $1b \cdot Fp^+$, and $1a^F \cdot Fp$.

Metric	^{31}P δ [ppm] ^[a]	$^1J_{\text{P,Se}}$ [Hz]	^{57}Fe δ [ppm] ^[b]	$d(\text{Fe}_1\text{--P}_1)$ [Å]	$\nu(\text{CO})$ [cm ^{−1}]	FIA [kcal mol ^{−1}] ^[c]	EDA-NOCV ^[d]							$\sigma(\text{P} \rightarrow \text{Fe})$	$\pi(\text{P} \leftarrow \text{Fe})$
							E_{tot}	E_{Pauli}	E_{estat}	E_{steric}	E_{disp}	E_{orb}			
1a	160.4	907 ^[e]	—	—	—	—	—	—	—	—	—	—	—	—	
1b	122.4	784 ^[e]	—	—	—	—	—	—	—	—	—	—	—	—	
1a ·Fp ⁺	183.5	—	616	2.1809(4)	2017, 2061	59.3	−91.9	122.7	−105.0	17.7	−16.1	−93.6	−61.7	−18.1	
1b ·Fp ⁺	141.4	—	688	2.2381(5)	2000, 2045	32.9	−99.8	130.0	−118.4	11.6	−18.4	−92.9	−65.8	−13.2	
1a ^F ·Fp	−3.0	—	1013	2.3047(9)	1952, 2007	—	—	—	—	—	—	—	—	—	

[a] ppm vs. 85% H_3PO_4 . [b] ppm vs. $Fe(CO)_5$. [c] Computed (M06L/def2-TZVP(CPCM:CH₂Cl₂)) according to the method in Ref. [32]. [d] EDA-NOCV computational results represent attractive and repulsive energies (kcal mol^{−1}) between the Fp^+ fragment and phosphorus ligands at the fragment geometry of the complex. The direction of donation is defined to be from phosphorus to iron. [e] Values from Ref. [25].

undertaken with the energy decomposition analysis–natural orbitals for chemical valence (EDA–NOCV) method^[30] as implemented in the ADF modeling program^[31] at the BP86/def2-TZVP level of density functional theory (Table 1, see Supporting Information for full details). Along lines described by Michalak,^[32] deconvolution of the covalent bonding portion (E_{orb}) into σ - and π -symmetry components for $\mathbf{1a}\cdot\text{Fp}^+$ gives donation $\sigma(\text{P}\rightarrow\text{Fe}) = -61.7 \text{ kcal mol}^{-1}$ (65.9% of E_{orb}) and back-donation $\pi(\text{P}\leftarrow\text{Fe}) = -18.1 \text{ kcal mol}^{-1}$ (19.3% of E_{orb}). An illustration of the electron deformation densities for the three principal NOCV interactions of $\mathbf{1a}\cdot\text{Fp}^+$ is presented in Figure 4. NOCV deformation density channel $\Delta\rho_1$ depicts depletion of electron density at P (red) and accrual of electron density at Fe (blue) as would be expected for an L-function σ -dative interaction. NOCV deformation density channels $\Delta\rho_2$ and $\Delta\rho_3$ correspond to the backflow of electron density from an Fe $d\pi$ orbital into P-based π -acceptor orbitals with two distinct interaction energies ($\Delta E^2_{\text{orb}} = -10.7 \text{ kcal mol}^{-1}$, $\Delta E^3_{\text{orb}} = -7.35 \text{ kcal mol}^{-1}$), consistent with the lifting of $p\pi$ degeneracy at nontrigonal $\mathbf{1a}$ shown by previous XAS evidence.^[21] By way of comparison, EDA–NOCV partitioning of the Fe–P bond in $\mathbf{1b}\cdot\text{Fp}^+$ gives donation $\sigma(\text{P}\rightarrow\text{Fe}) = -65.8 \text{ kcal mol}^{-1}$ (70.8% of E_{orb}) and back-donation $\pi(\text{P}\leftarrow\text{Fe}) = -13.2 \text{ kcal mol}^{-1}$ (14.2% of E_{orb}). This analysis therefore quantifies the relatively weaker σ -donating ability of nontrigonal $\sigma^3\text{-P}$ compound $\mathbf{1a}$ as compared to a compositionally related phosphorous triamide $\mathbf{1b}$ evident from spectroscopy (see above). Further, a combined consideration of the spectroscopic, structural, and theoretical data suggests a relatively stronger π -accepting ability of $\mathbf{1a}$ vs. $\mathbf{1b}$.

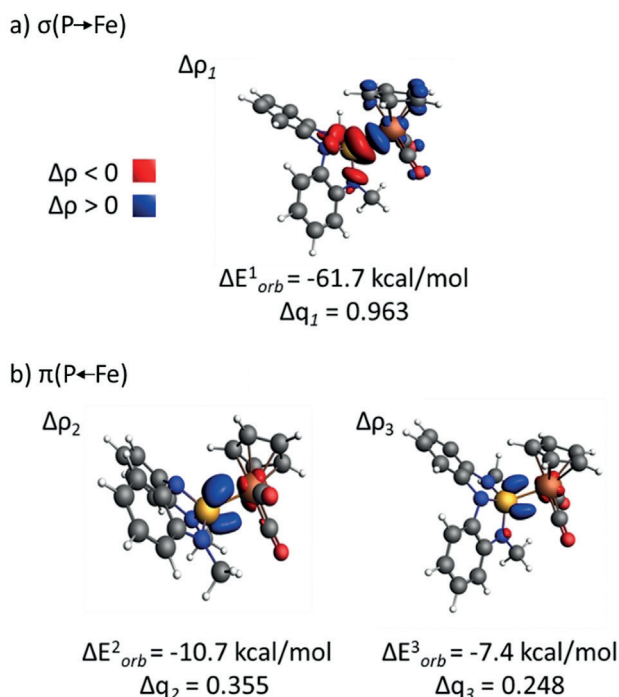


Figure 4. Contours of electron deformation density channels $\Delta\rho_1$, $\Delta\rho_2$, and $\Delta\rho_3$ describing the bonding between $\mathbf{1a}$ and the Fp^+ metal fragments with corresponding energies and charge estimations obtained from EDA–NOCV method.

To quantify the relative electrophilicity of P-based acceptor orbitals for $\mathbf{1a}\cdot\text{Fp}^+$ vs. $\mathbf{1b}\cdot\text{Fp}^+$, solvation-corrected fluoride ion affinities (FIAs) were computed at the M06L/def2-TZVP(CPCM:CH₂Cl₂) level of theory by isodesmic reaction enthalpies according to Christie's method.^[33] The FIA for $\mathbf{1a}\cdot\text{Fp}^+$ is computed to be significantly larger ($-\Delta H = 59.3 \text{ kcal mol}^{-1}$) than that for $\mathbf{1b}\cdot\text{Fp}^+$ ($-\Delta H = 32.9 \text{ kcal mol}^{-1}$). The low absolute values for the FIAs are indicative of a modest overall fluoride affinity,^[34] but the difference $\Delta(\text{FIA}) = 26.4 \text{ kcal mol}^{-1}$ conforms to the interpretation that P-based electrophilic reactivity should be favored at the nontrigonal complex $\mathbf{1a}\cdot\text{Fp}^+$.

The reactivity of $\mathbf{1a}\cdot\text{Fp}^+$ and $\mathbf{1b}\cdot\text{Fp}^+$ toward fluoride addition was probed experimentally. Treatment of compound $\mathbf{1a}\cdot\text{Fp}^+$ with tris(dimethylamino)sulfonium trimethyldifluoro-silicate (TASF) in acetonitrile resulted in an immediate change in color from yellow to deep orange (Figure 5 a). The formation of a single new phosphorus-containing species was evident by ^{31}P NMR spectroscopy, as indicated by the doublet resonance at $\delta = -3.0 \text{ ppm}$, which displayed large scalar coupling ($J = 971 \text{ Hz}$) consistent with the presence of a single fluorine bound to phosphorus via a direct P–F bond. The large upfield shift in ^{31}P NMR chemical shift is consistent with an increased coordination number at phosphorus by fluoride addition, and this inference is confirmed by observation of the complementary coupling in the lone ^{19}F NMR resonance ($\delta = 27.4 \text{ ppm}$, $J = 971 \text{ Hz}$, Figure 5 b). The product was thus assigned to be fluorometallophosphorane $\mathbf{1a}^{\text{F}}\cdot\text{Fp}$, in which a fluoride has been added to the phosphorus of $\mathbf{1a}\cdot\text{Fp}^+$ to generate a neutral complex. In solution, compound $\mathbf{1a}^{\text{F}}\cdot\text{Fp}$ exhibits time-averaged molecular C_s -symmetry with a persistent P–Fe bond; ^{13}C NMR spectra demonstrate an equivalence of the CO ligands (one resonance at $\delta = 211 \text{ ppm}$) with well-resolved $^2J_{\text{C-P}} = 49 \text{ Hz}$ and $^3J_{\text{C-F}} = 5.7 \text{ Hz}$ coupling constants. Treatment of $\mathbf{1b}\cdot\text{Fp}^+$ to identical fluorinating conditions (TASF, MeCN, rt) does not result in fluorination but instead returns starting materials alongside some decomposition of $\mathbf{1b}\cdot\text{Fp}^+$. It is evident that fluoride addition to a higher coordinate phosphorus ligand is enabled by the enhanced electrophilicity of $\mathbf{1a}\cdot\text{Fp}^+$ as compared to $\mathbf{1b}\cdot\text{Fp}^+$.

The air and moisture sensitive orange $\mathbf{1a}^{\text{F}}\cdot\text{Fp}$ can be crystallized by slow evaporation of a saturated CH₂Cl₂ solution at -35°C (Figure 5 c). X-ray diffractometry confirms the structural assignment of $\mathbf{1a}^{\text{F}}\cdot\text{Fp}$ as a metallophosphorane resulting from addition of an exogenous fluoride to $\sigma^3\text{-P}$ ligand $\mathbf{1a}$ without further substitution. With respect to the Fe bonding environment, compound $\mathbf{1a}^{\text{F}}\cdot\text{Fp}$ features an increased Fe–P bond length ($d_{\text{Fe-P}} = 2.3047(9) \text{ \AA}$) as compared to $\mathbf{1a}\cdot\text{Fp}^+$, as well as a shorter average Fe–C_{CO} bond length ($d_{\text{Fe-C}} = 1.764(3) \text{ \AA}$) that coincides with a bathochromic shift of the carbonyl stretching frequencies ($\nu_{\text{asym}} = 1952 \text{ cm}^{-1}$, $\nu_{\text{sym}} = 2007 \text{ cm}^{-1}$). With respect to the P bonding environment, metrical parameters give a geometry index of $\tau = 0.35$, indicating a geometry closer to that of a square pyramid than a trigonal bipyramid.^[35] The addition of fluoride results in an increase in all of the P–N bond lengths by $0.05 \text{ \AA} < \Delta d_{\text{P-N}} < 0.09 \text{ \AA}$ as is common for higher-coordinate main group compounds that compensate for their formal “hypervalent”

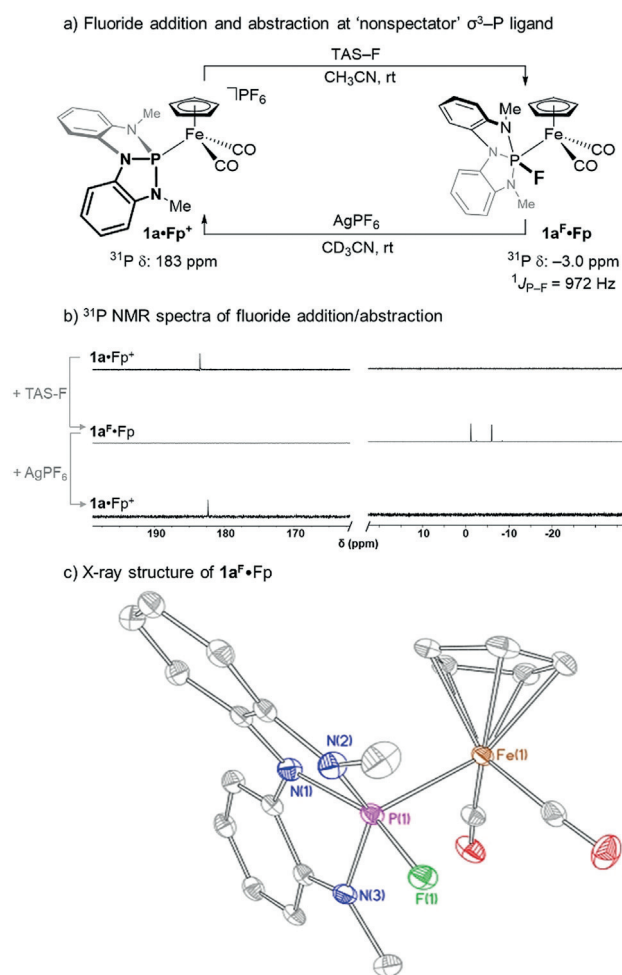


Figure 5. A) Reversible fluorination of $1\text{a}\cdot\text{Fp}^+$ and the resulting fluoro-metallophosphorane $1\text{a}^{\text{F}}\cdot\text{Fp}$. B) Solution ^{31}P NMR spectra in CD_3CN : (top) spectrum of $1\text{a}\cdot\text{Fp}^+$; (middle) spectrum of $1\text{a}^{\text{F}}\cdot\text{Fp}$ from addition of TAS-F to $1\text{a}\cdot\text{Fp}^+$; (bottom) spectrum of $1\text{a}\cdot\text{Fp}^+$ following treatment of $1\text{a}^{\text{F}}\cdot\text{Fp}$ with AgPF_6 and removal of precipitate (AgF). C) Thermal ellipsoid plot rendered at 50% probability level for $1\text{a}^{\text{F}}\cdot\text{Fp}$. Hydrogen atoms are removed for clarity. Relevant metrical data for $1\text{a}^{\text{F}}\cdot\text{Fp}$: $d(\text{Fe}-\text{P})$: 2.3047(9) Å, $d(\text{P}-\text{F})$: 1.6687(18) Å, $\angle(\text{N}_1-\text{P}-\text{F})$: 158.11(12)°, $\angle(\text{N}_2-\text{P}-\text{N}_3)$: 134.91(13)°, $\varphi(\text{C}_2-\text{Fe}-\text{P}-\text{F})$: 2.63°, $\varphi(\text{C}_1-\text{Fe}-\text{P}-\text{N}_3)$: 8.12°. See Supporting Information for full details.

character by distribution of electron density toward the substituents.^[36] The P-F bond length is quite long ($d_{\text{P-F}} = 1.6687(18)$ Å), but falls within the range ($1.64(11)$ Å $< d_{\text{P-F}} < 1.69(1)$ Å) observed for the only prior example of a structurally characterized fluorometallophosphorane (i.e. $\text{Ir}(\text{CO})\text{Cl}_2(\text{PEt}_3)_2(\text{PF}_4)$) from Holloway.^[37]

Bonding analysis in $1\text{a}\cdot\text{Fp}^+$ and $1\text{a}^{\text{F}}\cdot\text{Fp}$ reveals changes to the nature of the Fe-P σ -interactions as a function of fluoride binding. NBO analysis reports a dative covalent P \rightarrow Fe σ -interaction for $1\text{a}\cdot\text{Fp}^+$ described by an NLMO comprising modest polarization toward the phosphorus (P 56.2%/Fe 38.5%; Figure 6a, left) and involving a P donor NBO with $\text{sp}^{1.10}$ hybridization. The NLMO corresponding to the P-Fe bonding interaction in $1\text{a}^{\text{F}}\cdot\text{Fp}$ indicates an increased distribution across Fe-P (P 49.8%/Fe 43.9%; Figure 6b, left) with similar phosphorus parentage ($\text{sp}^{1.16}$). Moving from $1\text{a}\cdot\text{Fp}^+$ to $1\text{a}^{\text{F}}\cdot\text{Fp}$, the Wiberg bond indices decrease ($1\text{a}\cdot\text{Fp}^+$: WBI =

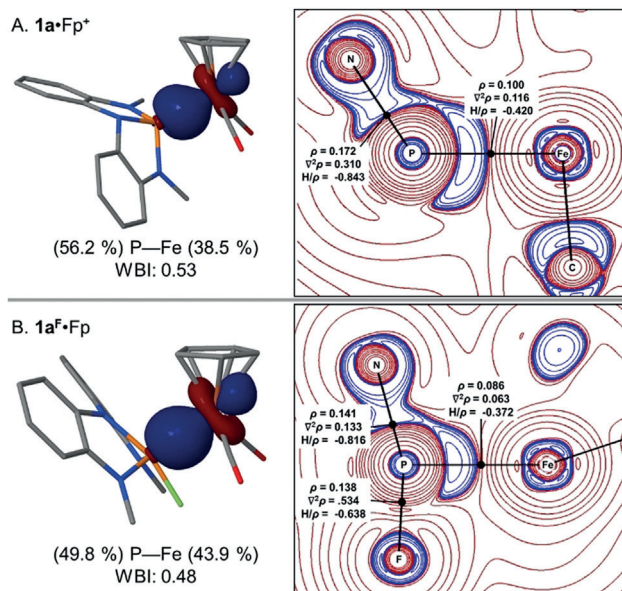


Figure 6. Bonding analysis for $1\text{a}\cdot\text{Fp}^+$ and $1\text{a}^{\text{F}}\cdot\text{Fp}$. A) Left: NLMO representing P-Fe bond for $1\text{a}\cdot\text{Fp}^+$. Right: Contour plot of the Laplacian of the electron-density topology $1\text{a}\cdot\text{Fp}^+$ in the plane containing the Fe, P, and N atoms. Areas of charge depletion are depicted in red and areas of charge concentration are depicted in blue. Black dots indicate bond critical points. Metrics represent relevant properties at the bond critical points (ρ in $\text{e}\text{\AA}^{-3}$, $\nabla^2\rho$ in $\text{e}\text{\AA}^{-5}$, H/ρ in atomic units). B) Left: NLMO representing P-Fe bond for $1\text{a}^{\text{F}}\cdot\text{Fp}$. Right: Contour plot of the Laplacian of the electron-density topology $1\text{a}^{\text{F}}\cdot\text{Fp}$ in the plane containing the Fe, P, and F atoms.

0.53; $1\text{a}^{\text{F}}\cdot\text{Fp}$: WBI = 0.48), in line with the observed increase in bond length from crystallography ($\Delta d_{\text{P-Fe}} = +0.12$ Å). For comparison, similar qualitative trends are reported by Gabbai for addition of fluoride to antimony in Pt-Sb bimetallics.^[38] Here, we invoke a decreased importance of π -backbonding effects in $1\text{a}^{\text{F}}\cdot\text{Fp}$ to account for this observation; the P-based acceptor orbital is saturated by addition of exogenous fluoride and unavailable for metal bonding.

Topological analysis of the computed electron density within the quantum theory of atoms in molecules (QTAIM) framework^[39] returns bond paths defined by (3, -1) critical points for P-Fe in $1\text{a}\cdot\text{Fp}^+$ (Figure 6a, right), and both P-Fe and P-F in $1\text{a}^{\text{F}}\cdot\text{Fp}$ (Figure 6b, right). No bond paths were located for any F \cdots Fe or N \cdots Fe trajectory, conforming to an η^1 -formulation of metallophosphorane $1\text{a}^{\text{F}}\cdot\text{Fp}$. Qualitatively, P-based valence shell charge concentrations are evident in the Laplacian of the electron density for both $1\text{a}\cdot\text{Fp}^+$ and $1\text{a}^{\text{F}}\cdot\text{Fp}$ along the P-Fe bond path, in line with an L- and X-function ligand classification, respectively. By contrast, the Laplacian distribution for the P-F bond is indicative of a "closed-shell interaction" and a dominant ionic contribution to the P-F bonding in $1\text{a}^{\text{F}}\cdot\text{Fp}$.

Consistent with the ionic character of the P-F bonding interaction, treatment of $1\text{a}^{\text{F}}\cdot\text{Fp}$ with fluoride abstracting reagents leads to removal of the F $^-$ ligand and regeneration of $1\text{a}\cdot\text{Fp}^+$. Specifically, the addition of 1 equiv of AgPF_6 to a CD_3CN solution of $1\text{a}^{\text{F}}\cdot\text{Fp}$ induces the orange solution to become yellow with immediate formation of precipitate. Following filtration, ^{31}P NMR spectroscopy (Figure 5b) con-

firms full consumption of $\mathbf{1a}^{\text{F-Fp}}$ and clean return of compound $\mathbf{1a}^{\text{Fp}^+}$. Evidently, both the nontrigonal phosphorus framework and the P–Fe bond are sufficiently robust as to be retained during the course of the nonspectator $\text{L} \rightarrow \text{X} \rightarrow \text{L}$ -switching cycle.

The data reported herein define the spectroscopic, structural, and electronic changes that accrue to phosphorus ligand $\mathbf{1a}$ as it undergoes increase in coordination number upon exogenous fluoride addition. The conversion from L- to X- function roles results in little change to the donor capacity of the phosphorus ligand, but the acceptor capacity is diminished. Further, the reversible nonspectator behavior of tricoordinate phosphorus ligand $\mathbf{1a}$ calls to mind recent developments for higher valent states of Sb ligands from Gabbaï.^[22] Given this periodic relationship within group 15, the broader implications of nonspectator L/X switching for phosphorus-based ligands in catalysis and sensing warrant further investigation.

Acknowledgements

Financial support was provided by NIH NIGMS (R21 GM134240). G.T.C. was supported by an NSF Graduate Research Fellowship. We thank Dr. Clemens Anklin (Bruker) for assistance with ^{57}Fe NMR studies and Drs. Charlene Tsay and Peter Müller (MIT) for assistance in crystallographic data collection.

Conflict of interest

The authors declare no conflict of interest.

Keywords: coordination modes · hypervalent compounds · ligand effects · ligand reactivity · phosphorous ligands

How to cite: *Angew. Chem. Int. Ed.* **2019**, 58, 15005–15009
Angew. Chem. **2019**, 131, 15147–15151

- [1] C. A. Tolman, *Chem. Rev.* **1977**, 77, 313–348.
- [2] R. H. Crabtree, *The Organometallic Chemistry of the Transition Metals*, Wiley, Hoboken, **2005**, pp. 87–124.
- [3] J. A. Gillespie, E. Zuidema, P. W. N. M. van Leeuwen, P. C. J. Kamer, *Phosphorus(III) Ligands in Homogenous Catalysis: Design and Synthesis*, Wiley, Hoboken, **2012**, pp. 1–26.
- [4] M. L. H. Green, *J. Organomet. Chem.* **1995**, 500, 127–148.
- [5] G. Parkin, in *Comprehensive Organometallic Chemistry III, Vol. 1* (Eds.: R. H. Crabtree, D. M. P. Mingos), Elsevier, Oxford, **2006**, Chapter 1.
- [6] L. Rosenberg, *Coord. Chem. Rev.* **2012**, 256, 606–626.
- [7] D. M. Roddick, B. D. Santarsiero, J. E. Bercaw, *J. Am. Chem. Soc.* **1985**, 107, 4670–4678.
- [8] M. D. Fryzuk, K. Bhangu, *J. Am. Chem. Soc.* **1988**, 110, 961–963.
- [9] J. Derrah, D. A. Pantazis, R. McDonald, L. Rosenberg, *Organometallics* **2007**, 26, 1473–1482.
- [10] M.-A. M. Hoyle, D. A. Pantazis, H. M. Burton, R. McDonald, L. Rosenberg, *Organometallics* **2011**, 30, 6458–6465.
- [11] Y.-E. Kim, S. Oh, S. Kim, O. Kim, J. Kim, S. W. Han, Y. Lee, *J. Am. Chem. Soc.* **2015**, 137, 4280–4283.
- [12] S. Oh, S. Kim, D. Lee, J. Gwak, Y. Lee, *Inorg. Chem.* **2016**, 55, 12863–12871.
- [13] S. Oh, Y. Lee, *Organometallics* **2016**, 35, 1586–1592.
- [14] A. M. Poitras, S. E. Knight, M. W. Bezpalko, B. M. Foxman, C. M. Thomas, *Angew. Chem. Int. Ed.* **2018**, 57, 1497–1500; *Angew. Chem.* **2018**, 130, 1513–1516.
- [15] J. Goodman, S. A. Macgregor, *Coord. Chem. Rev.* **2010**, 254, 1295–1306.
- [16] H. Nakazawa, K. Kubo, K. Miyoshi, *Bull. Chem. Soc. Jpn.* **2001**, 74, 2255–2267.
- [17] P. A. McLaughlin, J. G. Verkade, *Organometallics* **1998**, 17, 5937–5940.
- [18] K. Kubo, H. Nakazawa, T. Mizuta, K. Miyoshi, *Organometallics* **1998**, 17, 3522–3531.
- [19] K. Kubo, K. Bansho, H. Nakazawa, K. Miyoshi, *Organometallics* **1999**, 18, 4311–4316.
- [20] A. Tanushi, A. Radosevich, *J. Am. Chem. Soc.* **2018**, 140, 8114–8118.
- [21] K. Lee, A. V. Blake, A. Tanushi, S. M. McCarthy, D. Kim, S. M. Loria, C. M. Donahue, K. D. Spielvogel, J. M. Keith, S. R. Daly, A. T. Radosevich, *Angew. Chem. Int. Ed.* **2019**, 58, 6993–6998; *Angew. Chem.* **2019**, 131, 7067–7072.
- [22] For examples of high-valent heavier pnictogen ligands in catalysis and sensing, see: a) J. S. Jones, F. P. Gabbaï, *Acc. Chem. Res.* **2016**, 49, 857–867; b) J. S. Jones, C. R. Wade, F. P. Gabbaï, *Angew. Chem. Int. Ed.* **2014**, 53, 8876–8879; *Angew. Chem.* **2014**, 126, 9022–9025; c) D. You, F. P. Gabbaï, *J. Am. Chem. Soc.* **2017**, 139, 6843–6846; d) D. You, H. Yang, S. Sen, F. P. Gabbaï, *J. Am. Chem. Soc.* **2018**, 140, 9644–9651.
- [23] S. K. Chopra, J. C. Martin, *Heteroat. Chem.* **1991**, 2, 71–79.
- [24] M. P. Boone, D. W. Stephan, *Organometallics* **2014**, 33, 387–393.
- [25] D. Catheline, D. Astruc, *Organometallics* **1984**, 3, 1094–1100.
- [26] W. Zhao, S. M. McCarthy, T. Y. Lai, H. P. Yennawar, A. T. Radosevich, *J. Am. Chem. Soc.* **2014**, 136, 17634–17644.
- [27] Y.-C. Lin, E. Hatzakis, S. M. McCarthy, K. D. Reichl, T. Y. Lai, H. P. Yennawar, A. T. Radosevich, *J. Am. Chem. Soc.* **2017**, 139, 6008–6016.
- [28] R. Benn, H. Brenneke, A. Frings, H. Lehmkuhl, G. Mehler, A. Rufinska, T. Wildt, *J. Am. Chem. Soc.* **1988**, 110, 5661–5668.
- [29] R. M. Mampa, M. A. Fernandes, L. Carlton, *Organometallics* **2014**, 33, 3283–3299.
- [30] For recent overviews of EDA-NOCV, see: a) “The EDA Perspective of Chemical Bonding”: G. Frenking, F. M. Bickelhaupt, in *The Chemical Bond*, Wiley, Hoboken, **2014**, pp. 121–157; b) L. Zhao, M. von Hopfgarten, D. M. Andrada, G. Frenking, *WIREs Comput. Mol. Sci.* **2018**, 8, e1345.
- [31] ADF2018, SCM, Theoretical Chemistry, Vrije Universiteit, Amsterdam, The Netherlands, <http://www.scm.com>.
- [32] M. P. Mitoraj, A. Michalak, *Inorg. Chem.* **2010**, 49, 578–582.
- [33] K. O. Christe, D. A. Dixon, D. McLemore, W. W. Wilson, J. A. Sheehy, J. A. Boatz, *J. Fluorine Chem.* **2000**, 101, 151–153.
- [34] J. M. Slattery, S. Hussein, *Dalton Trans.* **2012**, 41, 1808–1815.
- [35] A. W. Addison, T. N. Rao, J. Reedijk, J. van Rijn, G. C. Verschoor, *J. Chem. Soc. Dalton Trans.* **1984**, 1349–1356.
- [36] R. H. Crabtree, *Chem. Soc. Rev.* **2017**, 46, 1720–1729.
- [37] A. J. Blake, R. W. Cockman, E. A. V. Ebsworth, S. G. D. Henderson, J. H. Holloway, N. J. Pilkington, D. W. H. Rankin, *Phosphorus Sulfur Relat. Elem.* **1987**, 30, 143–146.
- [38] J. S. Jones, C. R. Wade, F. P. Gabbaï, *Organometallics* **2015**, 34, 2647–2654.
- [39] R. Bader, *Atoms in Molecules: A Quantum Theory*, Oxford University Press, Oxford, **1990**.

Manuscript received: July 31, 2019

Accepted manuscript online: August 30, 2019

Version of record online: September 12, 2019